Spin-orbit-coupled spin-1 Bose-Einstein condensates in a toroidal trap: Even-petal-number necklacelike state and persistent flow

Keyan Liu, Huaxin He, Chenhui Wang, Yuanyuan Chen, and Yongping Zhang*

International Center of Quantum Artificial Intelligence for Science and Technology (QuArtist) and Department of Physics, Shanghai University, Shanghai 200444, China

(Received 26 September 2021; accepted 12 January 2022; published 28 January 2022)

Spin-orbit coupling has novel spin-flip symmetries, a spin-1 spinor Bose-Einstein condensate owns meaningful interactions, and a toroidal trap is topologically nontrivial. We incorporate the three together and study the ground-state phase diagram in a Rashba spin-orbit-coupled spin-1 Bose-Einstein condensate with a toroidal trap. The spin-flip symmetries give rise to two different interesting phases: persistent flows with a unit phase winding difference between three components, and necklace states with even petal number. The existing parameter regimes and properties of these phases are characterized by two-dimensional numerical calculations and an azimuthal analytical one-dimensional model.

DOI: 10.1103/PhysRevA.105.013323

I. INTRODUCTION

In atomic Bose-Einstein condensates (BECs), confinements play a key role in variously pertinent physics. One of the salient confining geometries is a toroidal trap. Considering macroscopic quantum property of BECs, periodic boundary imposed by the toroidal trap naturally gives rise to atomic persistent flows [1]. Experimental accessibility [1,2] makes that the toroidal BEC becomes a prototypical system to investigate superfluidity [3–8]. Furthermore, such confinement can be easily equipped with a rotation created by rotating a repulsive perturbation [9]. The response of superfluids to the rotation in a toroidal trap has been widely investigated [9–17].

The generalization of single-component toroidal BECs to multicomponents also draws much attention [18]. The population imbalance and fixed phase relation between multiple components bring persistent flows novel stability features [18–22]. It has been found that rich phase diagrams and interesting collective excitations can exist in interacting two-component [23–26] and three-component [27–29] toroidal BECs.

Each component behaves as a pseudospin state, therefore, two components correspond to spin-$\frac{1}{2}$ and three components can be explained as spin-1. Pseudospins can be arranged to couple with the external momentum, which leads to so-called spin-orbit coupling. It must be introduced into multicomponent BECs artificially [30]. The experimental realization of spin-orbit-coupled BECs represents a current advance in ultracold atomic physics [31–33]. The striking feature of spin-orbit-coupled BECs is the spontaneous emergence of striped density patterns [34–39]. The origination of stripes is that atoms condense simultaneously into multiple energy-minimum states. While, for a conventional condensate, atoms condense into only one energy minimum. Putting spin-orbit-coupled BECs in a toroidal trap quickly attracts interests [40–46]. The phase diagram of spin-orbit-coupled spin-$\frac{1}{2}$ BECs in a tight toroidal trap has been identified [41–43]. The nontrivial topology of the toroidal trap generates new features to striped patterns for Raman-induced spin-orbit coupling [41]. While Rashba spin-orbit coupling has same rotating symmetry as the toroidal trap, the density modulation for Rashba case is patterned along the azimuthal direction appearing as a necklace [42,43]. The most interesting is that such a necklacelike state has an odd number of petals [43]. It is also revealed that in Rashba spin-$\frac{1}{2}$ BECs both components can support persistent flows with a unit winding number difference between them [43]. Spin-orbit-coupled spin-1 BECs support more enriching phases. The effort in existing studies on spin-1 has been put into investigating the interplay between spin-orbit coupling and rotation [44–46]. The characteristics of phase diagram for spin-orbit-coupled spin-1 BECs with a toroidal confinement are still lacking. Considering the existence of the odd-petal-number necklace state in spin-$\frac{1}{2}$ system, it is natural to ask whether the necklace state still has specific petal number and what the persistent flow is in spin-1 BECs.

In this paper, we systematically characterize the ground-state phase diagram of a Rashba spin-orbit-coupled spin-1 BEC in a two-dimensional toroidal trap. The phases are identified from direct numerical calculations and an analytical study for a tight trap. When the toroidal trap is tight, the dynamics along the radial direction can be frozen, and the two-dimensional system is reduced to an one-dimensional effective model only considering the dynamics along the azimuthal direction. The effective model provides an analytical means to qualitatively understand two-dimensional numerical results. A spin-1 spinor BEC features density-density interaction and spin-spin interaction with respective strength c_0 and c_2 [47]. For an antiferromagnetic interaction $c_2 > 0$, depending on the spin-orbit coupling strength, there are two phases: persistent flows with the winding number $(-1, 0, 1)$ for three components and necklace states with even petal

*yongping11@t.shu.edu.cn

number. For a ferromagnetic interaction $c_2 < 0$, the ground state is a persistent flow, and there is always a unit winding number difference between three components. We find that the origination and properties of all phases relate to extraordinary spin-flip symmetries.

This paper is organized as follows. In Sec. II, we present the phase diagram from two-dimensional numerical calculations. Features of the persistent flow and necklace state are addressed by a spin-flip symmetry. In Sec. III, we develop an one-dimension analytical model to capture physics along the azimuthal direction. From the model, all phases are identified by using a variational wave function. A clear physical picture is provided for the existence and properties of ground states. Especially we address why the necklace state must have even petal number in a spin-1 BEC, while it would have odd number in a spin-$\frac{1}{2}$ analog. Sec. IV is the conclusion.

II. PHASE DIAGRAM

The experimental realization of Raman-induced spin-orbit coupling in a spin-1 BEC [48] stimulates the exploration of spin-orbit-coupled spinor BECs. Ground states and collective excitations of a homogeneously spin-orbit-coupled spin-1 BEC have been investigated theoretically [49–53]. With a toroidal trap, the system is described by the Gross–Pitaevskii equation (GPE) [44,52],

$$i\hbar\frac{\partial\Phi}{\partial t} = (H_{\rm sin} + H_{\rm int})\Phi. \tag{1}$$

The spinor wave function $\Phi = (\Phi_1, \Phi_2, \Phi_3)^T$ describes the occupation of three components. The single-particle Hamiltonian in Eq. (1) is

$$H_{\rm sin} = \frac{p_x^2 + p_y^2}{2m} + \lambda(F_x p_y - F_y p_x) + V(r), \tag{2}$$

with m being the mass of the atom. p_x and p_y are momenta along the x and y directions respectively. (F_x, F_y, F_z) are spin-1 Pauli matrices. The Rashba spin-orbit coupling is $\lambda(F_x p_y - F_y p_x)$ with the coupling strength λ. The external trap is two-dimensional toroidal, $V(r) = \frac{1}{2}m\omega_r^2(r - r_0)^2$, here $r^2 = x^2 + y^2$, the radius of torus is r_0, and ω_r is the trapping frequency. In the GPE, the nonlinear part is

$$H_{\rm int} = \begin{pmatrix} c_0\rho_0 + c_2\rho_z & c_2\rho_2 & 0 \\ c_2\rho_2^* & c_0\rho_0 & c_2\rho_2 \\ 0 & c_2\rho_2^* & c_0\rho_0 - c_2\rho_z \end{pmatrix}, \tag{3}$$

where $\rho_0 = |\Phi_1|^2 + |\Phi_2|^2 + |\Phi_3|^2$, $\rho_z = |\Phi_1|^2 - |\Phi_3|^2$, and $\rho_2 = \Phi_2^*\Phi_1 + \Phi_3^*\Phi_2$. The nonlinearity is characterized by the density-density interaction with the coefficient c_0 and spin-spin interaction with the coefficient c_2.

The GPE is quasi two dimensional since we consider a very tight trap along the z direction (i.e., the trap frequency ω_z is so large that the dynamics is frozen into the ground state of the trap). For convenience of numerical calculation, the GPE is dimensionless, we set the units of energy, length, time, and λ as $\hbar\omega_r$, $\sqrt{\hbar/m\omega_r}$, $1/\omega_r$, and $\sqrt{\hbar\omega_r/m}$, respectively. The wave function satisfies normalization condition, $\int dxdy(|\Phi_1|^2 + |\Phi_2|^2 + |\Phi_3|^2) = 1$. With these units, the nonlinear coefficients become $c_0 = 4N\sqrt{m\pi\omega_z/2\hbar}(2a_2 + a_0)/3$ and $c_2 = 4N\sqrt{m\pi\omega_z/2\hbar}(a_2 - a_0)/3$. Here, N is the atom number, and a_2 and a_0 are the s-wave scattering lengths in the total spin channels. We numerically find ground states by solving the GPE using the standard imaginary time evolution. The imaginary time evolution is implemented by the split-step Fourier method. In a detail calculation, the window of two-dimensional space is chosen as $(x, y) \in [-2\pi, 2\pi]$ and is discretized into a 256×256 grid. The radius of the trap maintains $r_0 = 4\sqrt{\hbar/m\omega_r}$.

Typical ground states for an antiferromagnetic interaction $c_2 > 0$ with different spin-orbit coupling strength λ are demonstrated in Fig. 1. There are two different phases. (1) When λ is small, three components distribute homogeneously in the ring [see Fig. 1(a)]. The first and third components share the same density, $|\Phi_1|^2 = |\Phi_3|^2$, and have an opposite-sign phase winding ± 1. These two components support persistent flows with a unit phase winding, while there is no phase winding in the second component. The existence of phase winding makes the size of the first and third components larger than that of the second component. (2) When λ is relatively large, the ground state becomes necklacelike patterns, which are shown in Figs. 1(b)–1(d). Three components have a same petal number. The density of the first component is same as that of the third component, $|\Phi_1|^2 = |\Phi_3|^2$. The petals in the second component do not spatially overlap with these in Φ_1 and Φ_3. The total density also shows a necklacelike geometry. These states are reminiscent of stripe phases from a homogeneous spin-orbit-coupled BEC. In homogeneous system, Rashba spin-orbit coupling can induce density stripes whose orientation is spontaneously chosen [34,37]. In the toroidal trap, the stripes are oriented along the azimuthal direction. Via this way, the boundaries of each petal in the necklace can be shortened for minimizing kinetic energy. The petal number increases as a function of λ. In Fig. 2, we show the dependence of petal number on λ and find that the petal number is always even and increases discontinuously with λ. The even-petal-number necklace state in spin-1 BECs is strikingly different from the only existing odd-number analog in spin-$\frac{1}{2}$ [43].

These two different ground states have two common features. From density and phase distributions in Fig. 1, we know that two ground states obey a same spin-flip symmetry $\hat{\mathcal{O}}$,

$$\hat{\mathcal{O}} = \mathcal{K}e^{i\pi F_y} = \mathcal{K}\begin{pmatrix} 0 & 0 & 1 \\ 0 & -1 & 0 \\ 1 & 0 & 0 \end{pmatrix}. \tag{4}$$

Here, $\mathcal{K}$ is the complex-conjugate operator, and $e^{i\pi F_y}$ is the operator to rotate spins by the angle of π along the F_y axis. The GPE and single-particle Hamiltonian $H_{\rm sin}$ have the symmetry $\hat{\mathcal{O}}$. Ground states inherit the symmetry and are its eigenstates with eigenvalue ± 1. This gives rise to

$$\Phi_1 = \pm\Phi_3^*, \quad \Phi_2 = \mp\Phi_2^*. \tag{5}$$

Therefore, the first and third components have a same density, and the wave function of the second component is purely real or imaginary. The other common feature is the phase separation between Φ_2 and Φ_1, Φ_3. The nonlinear part of the energy functional corresponding to the GPE is

$$E_{\rm non} = E_{\rm dd} + E_{\rm ss}, \tag{6}$$

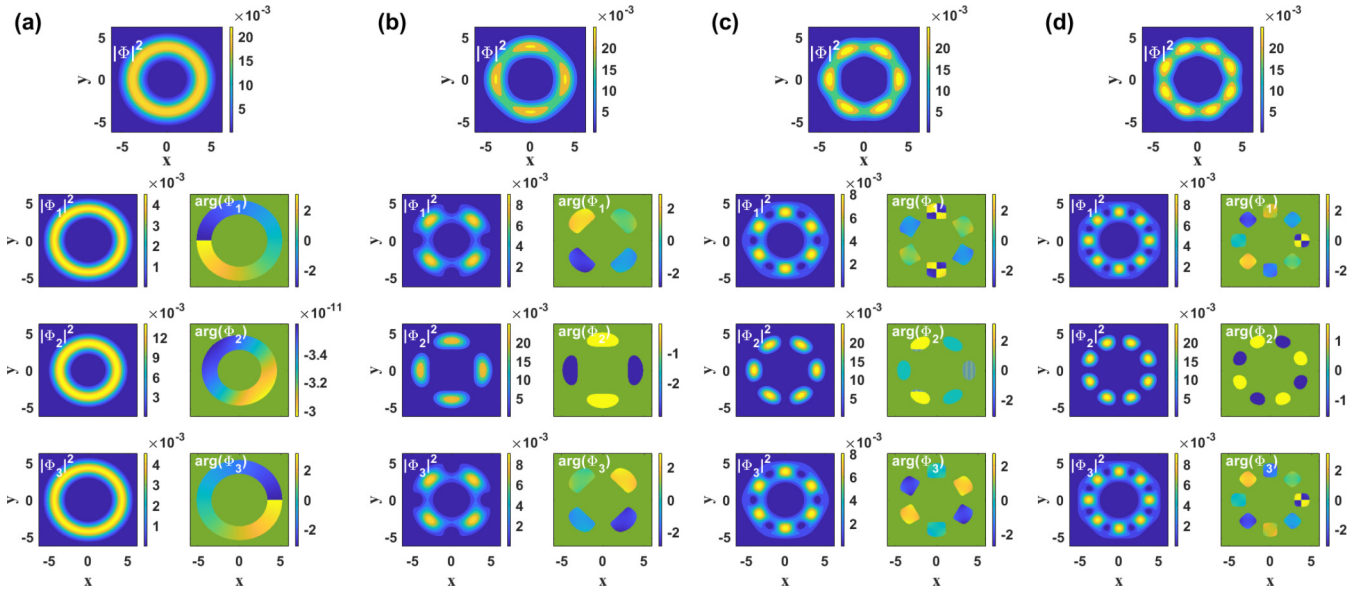

FIG. 1. Ground states with the antiferromagnetic interaction $c_2 = 1$ for different spin-orbit coupling strength λ. (a) $\lambda = 0.4\sqrt{\hbar\omega_r/m}$, (b) $\lambda = 0.6\sqrt{\hbar\omega_r/m}$, (c) $\lambda = 1.0\sqrt{\hbar\omega_r/m}$, (d) $\lambda = 1.2\sqrt{\hbar\omega_r/m}$. Other parameters are $r_0 = 4\sqrt{\hbar/m\omega_r}$ and $c_0 = 10$. In each block, the top panel is the total density distribution $|\Phi|^2 = |\Phi_1|^2 + |\Phi_2|^2 + |\Phi_3|^2$, followed by density distribution of each component on the left and corresponding phase distribution of each component on the right. The units of coordinates are $\sqrt{\hbar/m\omega_r}$.

where

$$E_{\rm dd} = \frac{c_0}{2}\int dxdy(|\Phi_1|^2 + |\Phi_2|^2 + |\Phi_3|^2)^2, \tag{7}$$

is the density-density interaction energy, and the spin-spin interaction energy is

$$\begin{aligned} E_{\rm ss} &= \frac{c_2}{2}\int dxdy[(\Phi^\dagger F_x\Phi)^2 + (\Phi^\dagger F_y\Phi)^2 + (\Phi^\dagger F_z\Phi)^2] \\ &= \frac{c_2}{2}\int dxdy\big[(|\Phi_1|^2 - |\Phi_3|^2)^2 + 2|\Phi_1|^2|\Phi_2|^2 \\ &\quad + 2|\Phi_2|^2|\Phi_3|^2 + \Phi_1\Phi_3\Phi_2^{*2} + \Phi_1^*\Phi_3^*\Phi_2^2\big]. \end{aligned} \tag{8}$$

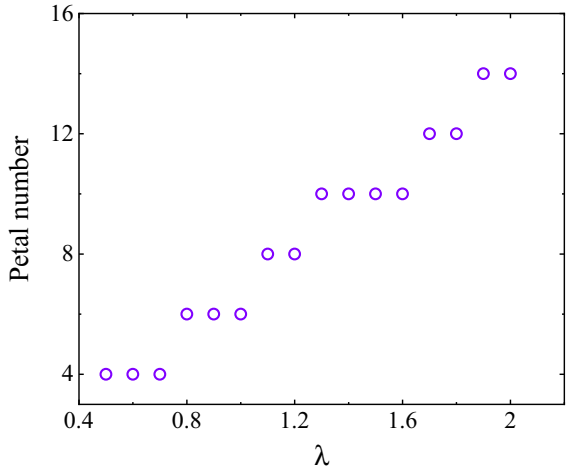

FIG. 2. The number of petals in the necklace state as a function of the spin-orbit coupling strength λ. It is found that the petal-number is always even. The other parameters are same as in Fig. 1. The units of λ are $\sqrt{\hbar\omega_r/m}$.

Substituting the symmetry result $\Phi_1 = \pm\Phi_3^*$, $\Phi_2 = \mp\Phi_2^*$ in Eq. (5) into the above energy functional, we immediately realize that ground states having the symmetry $\hat{\mathcal{O}}$ minimize the spin-spin interaction, i.e., $E_{\rm ss} = 0$. The density-density part becomes

$$\begin{aligned} E_{\rm dd} &= \frac{c_0}{2}\int dxdy(g_{11}|\Phi_1|^4 + g_{22}|\Phi_2|^4 + g_{12}|\Phi_1|^2|\Phi_2|^2), \\ g_{11} &= 4, \quad g_{22} = 1, \quad g_{12} = 4. \end{aligned} \tag{9}$$

It is interesting to note that the density-density part is similar to the interactions of a binary BEC. It is well known that a binary BEC features the phase separation when $g_{11}g_{22} < g_{12}^2$. According to this phase separation criterion, $E_{\rm dd}$ belongs to immiscible interactions, so Φ_1 and Φ_2 must be phase separated. For persistent flow states [as shown in Fig. 1(a)], Φ_2 and Φ_1, Φ_3 are spatially separated in the radial direction. While for necklace states, the separation is along the azimuthal direction [see Figs. 1(b)–1(d)].

The above is the ground state with an antiferromagnetic interaction, we find that for a ferromagnetic interaction $c_2 < 0$, it becomes different. Typical results with $c_2 = -1$ and different spin-orbit coupling strength λ are depicted in Fig. 3. The ground state always supports persistent flows and density distributes homogeneously along the azimuthal direction. Every component carries nonzero phase winding. The interesting thing is that there is always a unit phase winding difference between three components, which can be seen from the number of phase jumps in phase distributions in Fig. 3. The phase winding difference is also demonstrated from the size of density. For fixed parameters, the persistent flow with a large number of phase winding has a larger density size. In Fig. 3(a), for a small λ, the winding number for Φ_1, Φ_2, and Φ_3 are -3, -2, and -1, respectively, and the density size decreases. Increasing the spin-orbit coupling strength,

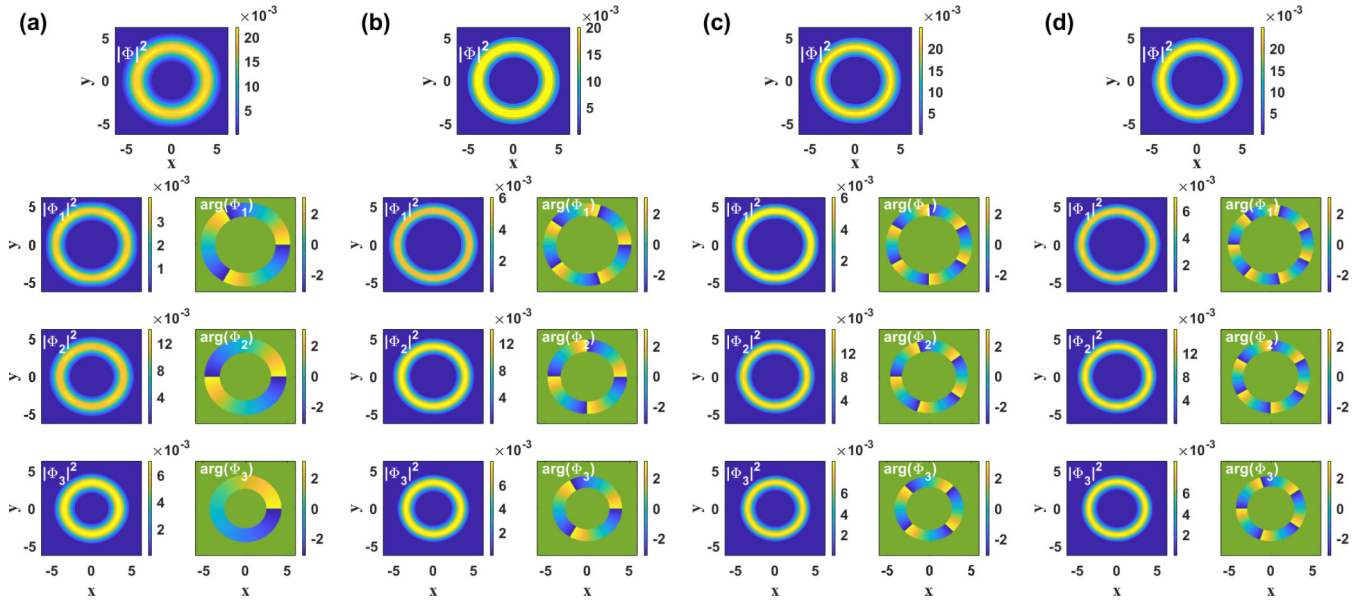

FIG. 3. Ground states with the ferromagnetic interaction $c_2 = -1$ for different spin-orbit coupling strength λ. (a) $\lambda = 0.6\sqrt{\hbar\omega_r/m}$, (b) $\lambda = 1.2\sqrt{\hbar\omega_r/m}$, (c) $\lambda = 1.6\sqrt{\hbar\omega_r/m}$, (d) $\lambda = 1.8\sqrt{\hbar\omega_r/m}$. Other parameters are $r_0 = 4\sqrt{\hbar/m\omega_r}$ and $c_0 = 10$. In each block, the top panel is the total density distribution $|\Phi|^2 = |\Phi_1|^2 + |\Phi_2|^2 + |\Phi_3|^2$, followed by density distribution of each component on the left and corresponding phase distribution of each component on the right. The units of coordinates are $\sqrt{\hbar/m\omega_r}$.

the phase winding in each component increases as shown in Figs. 3(b)–3(d). The dependence of the winding number in the second component on λ is demonstrated in Fig. 4. The winding number increases discontinuously as a function of λ.

In the literature, the ground state of a Rashba coupled spin-1 spinor BEC in the toroidal trap has been numerically studied in the antiferromagnetic regime in Refs. [44,46]. Especially, only four-times-petal-number necklace states are found [44]. Our phase diagram shows interesting characteristics. According to antiferromagnetic or ferromagnetic interactions, two different persistent flow states exist, and necklace states have even petal number. In the following, we develop an one-dimensional effective model to provide analytical insights into the existence of these states.

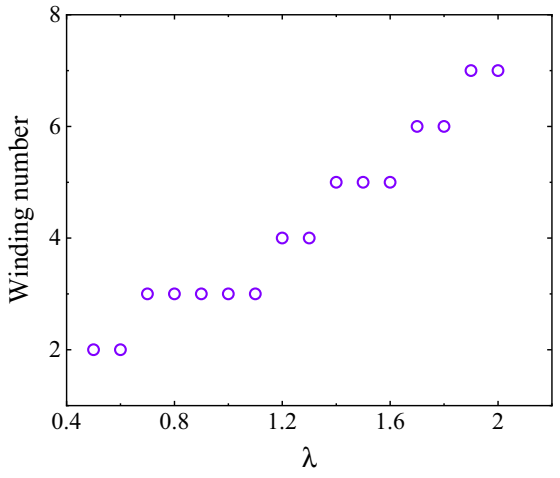

FIG. 4. The winding number of the second component as a function of λ. All parameters are same as in Fig. 3. The units of λ are $\sqrt{\hbar\omega_r/m}$.

III. EFFECTIVE MODEL

All above states reflect that the azimuthal effect plays an important role. We assume the toroidal trap is very tight, i.e., ω_r is a large scale. In this condition, the dynamics along the radial direction is frozen into the ground state of the harmonic trap. After integrating over the radial degree of freedom, the dynamics along the azimuthal direction would shine through [40,43,54]. The single-particle Hamiltonian in Eq. (2) reduces to one-dimensional $H_{\rm eff}$ which effectively describes the azimuthal effect [54],

$$H_{\rm eff} = \left(-i\frac{\partial}{\partial\phi}\right)^2 + \bar{\lambda}(\cos\phi F_x + \sin\phi F_y)\left(-i\frac{\partial}{\partial\phi}\right) - i\frac{\bar{\lambda}}{2}(\cos\phi F_y - \sin\phi F_x). \tag{10}$$

Here, ϕ is the azimuthal coordinate. $H_{\rm eff}$ is dimensionless, we use the unit of energy as $\hbar^2/(2mr_0^2)$, and $\bar{\lambda} = 2mr_0\lambda/\hbar$. After considering the nonlinear part in Eq. (3), the total energy becomes

$$E_{\rm tot} = \frac{1}{2\pi}\int_0^{2\pi} d\phi\left(\bar{\Phi}^\dagger H_{\rm eff}\bar{\Phi}\right) + \frac{\bar{c}_0}{4\pi}\int_0^{2\pi} d\phi|\bar{\Phi}|^4 + \frac{\bar{c}_2}{4\pi}\int_0^{2\pi} d\phi[(\bar{\Phi}^\dagger F_x\bar{\Phi})^2 + (\bar{\Phi}^\dagger F_y\bar{\Phi})^2 + (\bar{\Phi}^\dagger F_z\bar{\Phi})^2]. \tag{11}$$

Here, $\bar{c}_0 = 2mr_0^2/\hbar^2\sqrt{m\omega_r/(2\pi\hbar)}c_0$ and $\bar{c}_2 = 2mr_0^2/\hbar^2\sqrt{m\omega_r/(2\pi\hbar)}c_2$. The reduced wave function is $\bar{\Phi}(\phi) = (\bar{\Phi}_1(\phi), \bar{\Phi}_2(\phi), \bar{\Phi}_3(\phi))^T$, and $|\bar{\Phi}|^2 = |\bar{\Phi}_1|^2 + |\bar{\Phi}_2|^2 + |\bar{\Phi}_3|^2$.

The effective Hamiltonian $H_{\rm eff}$ conserves J_z with its definition being

$$J_z = -i\frac{\partial}{\partial\phi} + F_z, \tag{12}$$

i.e., $[J_z, H_{\rm eff}] = 0$. The conservation makes $H_{\rm eff}$ invariant under a rotation $U = \exp(i\theta J_z)$, where θ is an arbitrary angle. Therefore, $H_{\rm eff}$ and U have same eigenstates, which can be constructed from U as,

$$\bar{\Phi} = e^{in\phi}\begin{pmatrix} e^{-i\phi}\Phi_1' \\ \Phi_2' \\ e^{i\phi}\Phi_3' \end{pmatrix}, \tag{13}$$

where Φ_1', Φ_2', and Φ_3' are independent on ϕ. n is an integer and characterizes phase winding. Three components carry phase winding $(n-1, n, n+1)$. There is a unit phase winding difference between them. With the help of $\bar{\Phi}$, the effective Hamiltonian $H_{\rm eff}$ can be diagonalized to get eigenvalues $E(n)$, from which we immediately realize that $E(n) = E(-n)$. Physically, the degeneracy of $E(n)$ and $E(-n)$ originates from the symmetry $\hat{\mathcal{O}}$ defined in Eq. (4). Therefore, the lowest-energy state of the single-particle effective Hamiltonian $H_{\rm eff}$ is twofold degenerate.

The twofold-degenerate lowest-energy state offers an interesting accommodation for atoms to condense into. In the presence of the mean-field interactions, we construct the ground state ansatz by considering the superposition of the lowest energy state [38,52],

$$\bar{\Phi}^{(\rm gs)} = C_+\bar{\Phi}_n + C_-\hat{\mathcal{O}}\bar{\Phi}_n. \tag{14}$$

Here,

$$\bar{\Phi}_n = e^{in\phi}\begin{pmatrix} e^{-i\phi}\cos\alpha\cos\beta \\ -\sin\alpha \\ e^{i\phi}\cos\alpha\sin\beta \end{pmatrix}, \tag{15}$$

which is an eigenstate of $H_{\rm eff}$. The superposition coefficients C_+ and C_- satisfy $|C_+|^2 + |C_-|^2 = 1$. Substituting the trial wave function $\bar{\Phi}^{(\rm gs)}$ into the total energy $E_{\rm tot}$ in Eq. (11), we get $E_{\rm tot}(n, \alpha, \beta, C_+, C_-)$. All parameters n, α, β, C_+, and C_-, determining properties of the ground state, shall be fixed by minimizing the total energy $E_{\rm tot}$.

According to the resulting parameters from the minimization, the ground state has the following phases:

(1) For antiferromagnetic interactions $\bar{c}_2 > 0$, there are two phases. We take $\bar{c}_0 = 10$ and $\bar{c}_2 = 1$ as an example. (I) When $\bar{\lambda} \leqslant 0.86$, the results are $n = 0$, $\beta = 3\pi/4$, and one of the C_+ and C_- is zero, i.e., $C_+ = 0$, $C_- = 1$, or $C_+ = 1$, $C_- = 0$. With these parameters, it can be seen that $\hat{\mathcal{O}}\bar{\Phi}_{n=0} = -\bar{\Phi}_{n=0}$. $\bar{\Phi}_{n=0}$ and $\hat{\mathcal{O}}\bar{\Phi}_{n=0}$ are a same state up to a sign difference. The ground state supports persistent flows. The phase winding of three components is always -1, 0 and 1. $|\bar{\Phi}_1^{(\rm gs)}|^2 = |\bar{\Phi}_3^{(\rm gs)}|^2$, the size of which is always larger than that of $|\bar{\Phi}_2^{(\rm gs)}|^2$. This phase corresponds to the two-dimensional analog shown in Fig. 1(a). (II) When $\bar{\lambda} > 0.86$, results of the minimization are $n \neq 0$ and $C_+ = 1/\sqrt{2}$, $C_- = \pm 1/\sqrt{2}$. The ground state is the equal superposition of $\bar{\Phi}_n$ and $\hat{\mathcal{O}}\bar{\Phi}_n$, and thus is an eigenstate of $\hat{\mathcal{O}}$. Because of the superposition, the density of the ground state is periodically modulated along the azimuthal direction, $|\bar{\Phi}_1^{(\rm gs)}|^2 = |\bar{\Phi}_3^{(\rm gs)}|^2 = \cos^2\alpha[1 \pm \sin(2\beta)\cos(2n\phi)]$, $|\bar{\Phi}_2^{(\rm gs)}|^2 = 2\sin^2\alpha[1 - \cos(2n\phi)]$, here $\pm$ depends on the sign of C_-. Such density modulated ground states correspond to necklace states found in Figs. 1(b)–1(d). The nature of necklace states is that the period of three components is same and is an even number $2n$.

(2) For ferromagnetic interactions $\bar{c}_2 < 0$, the minimization always chooses $C_+ = 0, C_- = 1$ or $C_+ = 1, C_- = 0$. The ground state is a persistent flow with phase winding number $(n-1, n, n+1)$ or $(-n-1, -n, -n+1)$ for three components. These two configurations are spontaneously chosen. The unique feature of such ground state is that there is a unit phase winding difference between three components. These states correspond to two-dimensional persistent flows found in Fig. 3, where only the configuration $(-n-1, -n, -n+1)$ is shown.

The possible existence of the even-petal-number necklace state in spin-1 BECs is due to the cooperation of symmetries $\hat{\mathcal{O}}$ and J_z. It is interesting to compare with a spin-$\frac{1}{2}$ system, where only the odd-petal-number state can exist. The effective azimuthal Hamiltonian for a Rashba coupled spin-$\frac{1}{2}$ is

$$H_{\rm eff}' = \left(-i\frac{\partial}{\partial\phi}\right)^2 + \bar{\lambda}(\cos\phi\sigma_x + \sin\phi\sigma_y)\left(-i\frac{\partial}{\partial\phi}\right) - i\frac{\bar{\lambda}}{2}(\cos\phi\sigma_y - \sin\phi\sigma_x), \tag{16}$$

which is similar to Eq. (10), but replacing spin-1 matrices F by spin-$\frac{1}{2}$ Pauli matrices σ [40,43]. The conservation of

$$J_z' = -i\partial/\partial\phi + \sigma_z/2, \tag{17}$$

for $H_{\rm eff}'$ requires its eigenstates as

$$\bar{\Phi}_n' = e^{in\phi}\begin{pmatrix} \Phi_1' \\ e^{i\phi}\Phi_2' \end{pmatrix}. \tag{18}$$

The symmetry

$$\hat{\mathcal{O}}' = \mathcal{K}e^{i\pi\sigma_y/2}, \tag{19}$$

gives rise to the degeneracy of $\bar{\Phi}_n'$ and $\hat{\mathcal{O}}'\bar{\Phi}_n'$. Therefore, the possible ground state is the superposition of $\bar{\Phi}_n'$ and $\hat{\mathcal{O}}'\bar{\Phi}_n'$ with the corresponding density $\propto\cos[(2n+1)\phi]$. The necklace state in the spin-$\frac{1}{2}$ system takes an odd petal number. It is noting that there is a $\frac{1}{2}$ in the symmetries $\hat{\mathcal{O}}'$ and J_z', which is due to the SU(2) nature of spin-$\frac{1}{2}$ spins. This unique SU(2) property makes petal number in necklace states of a spin-$\frac{1}{2}$ BEC odd.

At last, we would like to address the effect of the quadratic Zeeman coupling on above results. The quadratic Zeeman coupling plays an important role in spin-1 spinor BECs [47]. It is qF_z^2, which should be incorporated into $H_{\rm sin}$ in Eq. (2) and $H_{\rm eff}$ in Eq. (10). Here, q describes the strength of the quadratic Zeeman term. In the Raman-induced spin-orbit-coupled spin-1 BEC experiment, it can be tuned [48]. It is interesting to find that the quadratic Zeeman term does not destroy the symmetries $\hat{\mathcal{O}}$ and J_z. Therefore, its existence does not qualitatively change the results from two-dimensional numerical calculations and from the one-dimensional analytical model. We find that it just slightly modifies the demarcation between the persistent flow and necklace state for antiferromagnetic interactions. In Fig. 5, we show the dependence of the critical spin-orbit coupling strength $\bar{\lambda}_c$ on the quadratic Zeeman effect q. For antiferromagnetic interactions, when $|\bar{\lambda}| < |\bar{\lambda}_c|$, the ground state is a persistent flow with $n = 0$ [see Eq. (15)],

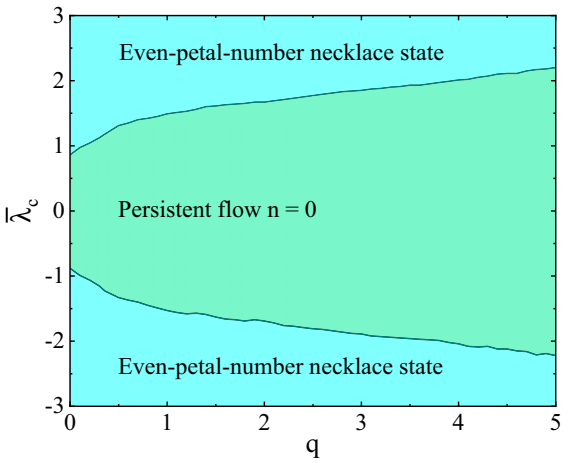

FIG. 5. The critical value of the spin-orbit coupling strength $\bar{\lambda}_c$ between the persistent flow and necklace state as a function of the quadratic Zeeman effect q for an antiferromagnetic interaction $\bar{c}_2 = 1$ from the one-dimensional effective model. The other parameter is $\bar{c}_2 = 10$.

when $|\bar{\lambda}| > |\bar{\lambda}_c|$, the ground state is an even-petal-number necklace state. There is a slight increase of $|\bar{\lambda}_c|$ as a function of q. We also note that in Fig. 5 there is a symmetry between $\bar{\lambda} > 0$ and $\bar{\lambda} < 0$, this is because that the effective Hamiltonian $H_{\text{eff}} + qF_z^2$ has a spin rotation symmetry $e^{i\pi F_z}$, the physics in the $\bar{\lambda} < 0$ regime is the same as that in the regime of $\bar{\lambda} > 0$.

We conclude that it is the symmetries $\hat{\mathcal{O}}$ and J_z that leads to the existence of the persistent flow and necklace state. Both symmetries are unique properties of the Rashba spin-orbit coupling. Raman-induced spin-orbit coupling does not have them, therefore, the ground state should be very different from our results. In experiments, the Raman-induced spin-orbit coupling can be accessed much easier than the Rashba spin-orbit coupling [48]. The experimental realization of the Rashba spin-orbit coupling is only in a spin-$\frac{1}{2}$ BEC [32]. Its realization in a spin-1 spinor BEC is still an experimental challenge.

IV. CONCLUSION

We systematically study the ground-state phase diagram in a Rashba spin-orbit-coupled spin-1 BEC trapped in a two-dimensional toroidal trap. The spin-flip symmetries of the spin-orbit coupling endow new features to the persistent flow and support the even-petal-number necklace state. The chosen phases depend on the sign of the spinor's spin-spin interaction. The toroidal trapped spin-orbit-coupled BEC provides a versatile playground to investigate necklace states. They emerge as ground states with spontaneous breaking of the continuous rotation symmetry. Therefore, they are always dynamically stable, which is in favor of experimental observation. The petal number of the necklace state can be tuned by changing the spin-orbit coupling strength. The number is always odd in spin-$\frac{1}{2}$ BECs, while it is even in spin-1 systems.

ACKNOWLEDGMENTS

This work is supported by National Natural Science Foundation of China with Grants No. 11974235 and No. 11774219.

[1] C. Ryu, M. F. Andersen, P. Cladé, V. Natarajan, K. Helmerson, and W. D. Phillips, Observation of Persistent Flow of a Bose-Einstein Condensate in a Toroidal Trap, Phys. Rev. Lett. **99**, 260401 (2007).

[2] A. Ramanathan, K. C. Wright, S. R. Muniz, M. Zelan, W. T. Hill, C. J. Lobb, K. Helmerson, W. D. Phillips, and G. K. Campbell, Superflow in a Toroidal Bose-Einstein Condensate: an Atom Circuit with a Tunable Weak Link, Phys. Rev. Lett. **106**, 130401 (2011).

[3] P. Mason and N. G. Berloff, Dynamics of quantum vortices in a toroidal trap, Phys. Rev. A **79**, 043620 (2009).

[4] A. V. Yulin, Y. V. Bludov, V. V. Konotop, V. Kuzmiak, and M. Salerno, Superfluidity of Bose-Einstein condensates in toroidal traps with nonlinear lattices, Phys. Rev. A **84**, 063638 (2011).

[5] S. Baharian and G. Baym, Bose-Einstein condensates in toroidal traps: Instabilities, swallow-tail loops, and self-trapping, Phys. Rev. A **87**, 013619 (2013).

[6] A. Kumar, S. Eckel, F. Jendrzejewski, and G. K. Campbell, Temperature-induced decay of persistent currents in a superfluid ultracold gas, Phys. Rev. A **95**, 021602(R) (2017).

[7] J. Polo, R. Dubessy, P. Pedri, H. Perrin, and A. Minguzzi, Oscillations and Decay of Superfluid Currents in a One-Dimensional Bose Gas on a Ring, Phys. Rev. Lett. **123**, 195301 (2019).

[8] M. Kunimi and I. Danshita, Decay mechanisms of superflow of Bose-Einstein condensates in ring traps, Phys. Rev. A **99**, 043613 (2019).

[9] S. Eckel, J. G. Lee, F. Jendrzejewski, N. Murray, C. W. Clark, C. J. Lobb, W. D. Phillips, M. Edwards, and G. K. Campbell, Hysteresis in a quantized superfluid 'atomtronic' circuit, Nature (London) **506**, 200 (2014).

[10] A. Aftalion and P. Mason, Rotation of a Bose-Einstein condensate held under a toroidal trap, Phys. Rev. A **81**, 023607 (2010).

[11] R. Dubessy, T. Liennard, P. Pedri, and H. Perrin, Critical rotation of an annular superfluid Bose-Einstein condensate, Phys. Rev. A **86**, 011602(R) (2012).

[12] A. White, T. Hennessy, and T. Busch, Emergence of classical rotation in superfluid Bose-Einstein condensates, Phys. Rev. A **93**, 033601 (2016).

[13] A. Roussou, J. Smyrnakis, M. Magiropoulos, N. K. Efremidis, and G. M. Kavoulakis, Rotating Bose-Einstein condensates with a finite number of atoms confined in a ring potential: Spontaneous symmetry breaking beyond the mean-field approximation, Phys. Rev. A **95**, 033606 (2017).

[14] A. Muñoz Mateo, V. Delgado, M. Guilleumas, R. Mayol, and J. Brand, Nonlinear waves of Bose-Einstein condensates in rotating ring-lattice potentials, Phys. Rev. A **99**, 023630 (2019).

[15] A. Pérez-Obiol and T. Cheon, Bose-Einstein condensate confined in a one-dimensional ring stirred with a rotating delta link, Phys. Rev. E **101**, 022212 (2020).

[16] B. Eller, O. Oladehin, D. Fogarty, C. Heller, C. W. Clark, and M. Edwards, Producing flow in racetrack atom circuits by stirring, Phys. Rev. A **102**, 063324 (2020).

[17] E. Arabahmadi, D. Schumayer, and D. A. W. Hutchinson, Universal nomogram for the atomtronic quantum rotation sensor, Phys. Rev. A **103**, 043319 (2021).

[18] S. Beattie, S. Moulder, R. J. Fletcher, and Z. Hadzibabic, Persistent Currents in Spinor Condensates, Phys. Rev. Lett. **110**, 025301 (2013).

[19] J. Smyrnakis, S. Bargi, G. M. Kavoulakis, M. Magiropoulos, K. Kärkkäinen, and S. M. Reimann, Mixtures of Bose Gases Confined in a Ring Potential, Phys. Rev. Lett. **103**, 100404 (2009).

[20] S. Bargi, F. Malet, G. M. Kavoulakis, and S. M. Reimann, Persistent currents in Bose gases confined in annular traps, Phys. Rev. A **82**, 043631 (2010).

[21] K. Anoshkin, Z. Wu, and E. Zaremba, Persistent currents in a bosonic mixture in the ring geometry, Phys. Rev. A **88**, 013609 (2013).

[22] M. Abad, A. Sartori, S. Finazzi, and A. Recati, Persistent currents in two-component condensates in a toroidal trap, Phys. Rev. A **89**, 053602 (2014).

[23] T. Shimodaira, T. Kishimoto, and H. Saito, Connection between rotation and miscibility in a two-component Bose-Einstein condensate, Phys. Rev. A **82**, 013647 (2010).

[24] Z. Wu, E. Zaremba, J. Smyrnakis, M. Magiropoulos, N. K. Efremidis, and G. M. Kavoulakis, Mean-field yrast spectrum and persistent currents in a two-component Bose gas with interaction asymmetry, Phys. Rev. A **92**, 033630 (2015).

[25] Z. Chen, Y. Li, N. P. Proukakis, and B. A. Malomed, Immiscible and miscible states in binary condensates in the ring geometry, New J. Phys. **21**, 073058 (2019).

[26] A. Roussou, J. Smyrnakis, M. Magiropoulos, N. K. Efremidis, G. M. Kavoulakis, P. Sandin, M. Ögren, and M. Gulliksson, Excitation spectrum of a mixture of two Bose gases confined in a ring potential with interaction asymmetry, New J. Phys. **20**, 045006 (2018).

[27] H. Mäkelä and E. Lundh, Excitation spectrum of a toroidal spin-1 Bose-Einstein condensate, Phys. Rev. A **88**, 033622 (2013).

[28] A. I. Yakimenko, K. O. Isaieva, S. I. Vilchinskii, and M. Weyrauch, Stability of persistent currents in spinor Bose-Einstein condensates, Phys. Rev. A **88**, 051602(R) (2013).

[29] M. Kunimi, Metastable spin textures and Nambu-Goldstone modes of a ferromagnetic spin-1 Bose-Einstein condensate confined in a ring trap, Phys. Rev. A **90**, 063632 (2014).

[30] D. L. Campbell, G. Juzeliūnas, and I. B. Spielman, Realistic Rashba and Dresselhaus spin-orbit coupling for neutral atoms, Phys. Rev. A **84**, 025602 (2011).

[31] Y. J. Lin, K. Jiménez-García, and I. B. Spielman, Spin-orbit-coupled Bose–Einstein condensates, Nature (London) **471**, 83 (2011).

[32] Z. Wu, L. Zhang, W. Sun, X.-T. Xu, B.-Z. Wang, S.-C. Ji, Y. Deng, S. Chen, X.-J. Liu, and J.-W. Pan, Realization of two-dimensional spin-orbit coupling for Bose-Einstein condensates, Science **354**, 83 (2016).

[33] C. Hamner, Y. Zhang, M. A. Khamehchi, M. J. Davis, and P. Engels, Spin-Orbit-Coupled Bose-Einstein Condensates in a One-Dimensional Optical Lattice, Phys. Rev. Lett. **114**, 070401 (2015).

[34] C. Wang, C. Gao, C.-M. Jian, and H. Zhai, Spin-Orbit Coupled Spinor Bose-Einstein Condensates, Phys. Rev. Lett. **105**, 160403 (2010).

[35] T.-L. Ho and S. Zhang, Bose-Einstein Condensates with Spin-Orbit Interaction, Phys. Rev. Lett. **107**, 150403 (2011).

[36] H. Hu, B. Ramachandhran, H. Pu, and X.-J. Liu, Spin-Orbit Coupled Weakly Interacting Bose-Einstein Condensates in Harmonic Traps, Phys. Rev. Lett. **108**, 010402 (2012).

[37] Y. Zhang, L. Mao, and C. Zhang, Mean-Field Dynamics of Spin-Orbit Coupled Bose-Einstein Condensates, Phys. Rev. Lett. **108**, 035302 (2012).

[38] Y. Li, L. P. Pitaevskii, and S. Stringari, Quantum Tricriticality and Phase Transitions in Spin-Orbit Coupled Bose-Einstein Condensates, Phys. Rev. Lett. **108**, 225301 (2012).

[39] J.-R. Li, J. Lee, W. Huang, S. Burchesky, B. Shteynas, F. C. Top, A. O. Jamison, and W. Ketterle, A stripe phase with supersolid properties in spin-orbit-coupled Bose-Einstein condensates, Nature (London) **543**, 91 (2017).

[40] O. Fialko, J. Brand, and U. Zülicke, Soliton magnetization dynamics in spin-orbit-coupled Bose-Einstein condensates, Phys. Rev. A **85**, 051605(R) (2012).

[41] E. O. Karabulut, F. Malet, A. L. Fetter, G. M. Kavoulakis, and S. M. Reimann, Spin-orbit-coupled Bose-Einstein-condensed atoms confined in annular potentials, New J. Phys. **18**, 015013 (2016).

[42] X.-F. Zhang, M. Kato, W. Han, S.-G. Zhang, and H. Saito, Spin-orbit-coupled Bose-Einstein condensates held under a toroidal trap, Phys. Rev. A **95**, 033620 (2017).

[43] A. C. White, Y. Zhang, and T. Busch, Odd-petal-number states and persistent flows in spin-orbit-coupled Bose-Einstein condensates, Phys. Rev. A **95**, 041604(R) (2017).

[44] J.-G. Wang, L.-L. Xu, and S.-J. Yang, Ground-state phases of the spin-orbit-coupled spin-1 Bose gas in a toroidal trap, Phys. Rev. A **96**, 033629 (2017).

[45] H. Wang, L. Wen, H. Yang, C. Shi, and J. Li, Vortex states and spin textures of rotating spin-orbit-coupled Bose-Einstein condensates in a toroidal trap, J. Phys. B: At., Mol. Opt. Phys. **50**, 155301 (2017).

[46] P. Peng, G.-Q. Li, W.-L. Yang, and Z.-Y. Yang, Exotic ground states of a spin-orbit-coupled spinor Bose-Einstein condensate trapped by a toroidal potential, Laser Phys. Lett. **15**, 085501 (2018).

[47] Y. Kawaguchi and M. Ueda, Spinor Bose–Einstein condensates, Phys. Rep. **520**, 253 (2012).

[48] D. L. Campbell, R. M. Price, A. Putra, A. Valdés-Curiel, D. Trypogeorgos, and I. B. Spielman, Magnetic phases of spin-1 spin–orbit-coupled Bose gases, Nat. Commun. **7**, 10897 (2016).

[49] Z. Lan and P. Öhberg, Raman-dressed spin-1 spin-orbit-coupled quantum gas, Phys. Rev. A **89**, 023630 (2014).

[50] S. S. Natu, X. Li, and W. S. Cole, Striped ferronematic ground states in a spin-orbit-coupled $s = 1$ Bose gas, Phys. Rev. A **91**, 023608 (2015).

[51] Z.-Q. Yu, Phase transitions and elementary excitations in spin-1 Bose gases with Raman-induced spin-orbit coupling, Phys. Rev. A **93**, 033648 (2016).

[52] K. Sun, C. Qu, Y. Xu, Y. Zhang, and C. Zhang, Interacting spin-orbit-coupled spin-1 Bose-Einstein condensates, Phys. Rev. A **93**, 023615 (2016).

[53] G. I. Martone, F. V. Pepe, P. Facchi, S. Pascazio, and S. Stringari, Tricriticalities and Quantum Phases in Spin-Orbit-Coupled Spin-1 Bose Gases, Phys. Rev. Lett. **117**, 125301 (2016).

[54] F. E. Meijer, A. F. Morpurgo, and T. M. Klapwijk, One-dimensional ring in the presence of Rashba spin-orbit interaction: Derivation of the correct Hamiltonian, Phys. Rev. B **66**, 033107 (2002).